JOURNAL OF THERMOPHYSICS AND HEAT TRANSFER
Vol. 22, No. 3, July–September 2008

Boltzmann and Master Equations for Magnetohydrodynamics in Weakly Ionized Gases

Gianpiero Colonna*
Consiglio Nazionale delle Ricerche, 70126 Bari, Italy
and
Mario Capitelli†
Universita di Bari, 70126 Bari, Italy

DOI: 10.2514/1.33479

A self-consistent model for heavy particles (state-to-state master equations) and for free electrons (Boltzmann equation) is presented. The kinetic model was coupled with a fluid dynamics code for quasi-one-dimensional nozzle flow interacting with external electric and magnetic fields. The amplitude of the electric field is controlled by considering a power supply with resistance to limit circuit current. The model can consider any configuration of the fields and it takes into account tensorial electron mobility. Results for argon supersonic expansion are obtained for different field configurations.

Nomenclature

A	=	nozzle section
$\mathbf{A}$	=	$-(e/m_e)\mathbf{E} + \mathbf{g}$
$\dot{A}_{sul}$	=	Einstein coefficient for the sth species in the $u \rightarrow l$ transition
$\mathbf{a}$	=	acceleration term in the Boltzmann equation
$\mathbf{B}$	=	magnetic field
c^{pr}	=	product stoichiometric coefficients
c^{re}	=	reactant stoichiometric coefficients
$\mathbf{d}$	=	vector of distance between electrodes, with the same verse and direction as $\mathbf{E}$
$\mathbf{E}$	=	electric field
$\mathbf{E}_{\mathrm{F}}$	=	Faraday electromotive field
e	=	proton charge, C
$\mathbf{F}_{\mathrm{MHD}}$	=	magnetohydrodynamic interaction
F_x	=	component of the external force in the flow direction
f	=	electron distribution in phase space
f_{sv}	=	internal level distribution function
f_0	=	isotropic part of the electron velocity distribution
$\mathbf{f}_1$	=	anisotropic part of the electron velocity distribution
$\mathbf{g}$	=	gravitational acceleration
g_i^s	=	statistical weight of the ith level of the sth species
H_s^f	=	molar formation enthalpy
h	=	Plank constant
h_{in}	=	internal enthalpy
h_T	=	thermal enthalpy
I	=	current intensity
$\hat{I}$	=	identity matrix
$\mathbf{J}$	=	current density
J_{ee}	=	electron–electron collision flux term for the Boltzmann equation
J_{el}	=	elastic collision flux term for the Boltzmann equation
J_f	=	external fields flux term for the Boltzmann equation
J_{ne}	=	expansion flux term for the Boltzmann equation
j_{Hall}	=	Hall current density
$\mathcal{K}$	=	pseudoconstants for the Euler equation
K_{eq}	=	equilibrium constant
k	=	Boltzmann constant
L_s	=	number of internal levels
$\hat{M}$	=	kinetic matrix
$\bar{m}$	=	mean molar mass
m_e	=	electron mass
N	=	heavy-particle density
N_e	=	electron density
N_i	=	density of the ith species
N_{su}	=	population density for the sth species in the uth level
n_0	=	electron energy distribution function
$\mathbf{n}_1$	=	anisotropic part of the electron energy distribution function
P	=	gas pressure
$\dot{Q}$	=	energy density production rate
$\dot{Q}_J$	=	energy density production rate due to Joule heating
$\dot{Q}_{\mathrm{rad}}$	=	energy density loss rate due to spontaneous emission
Q_s	=	internal partition function of sth species
$\mathbf{Q}_0$	=	driving force for the anisotropic part of the electron distribution
$\mathbf{R}$	=	$-(e/m_e)\mathbf{B}$
R_c	=	circuit resistance
R_p	=	rate constant
$R^\star$	=	ideal-gas constant$/\bar{m}$
$\mathbf{r}$	=	position vector
S_e	=	transversal section of the electrodes
S_{in}	=	inelastic collision source term for the Boltzmann equation
S_{ion}	=	ionization collision source term for the Boltzmann equation
$\bar{S}_{\mathrm{LC}}$	=	operator to calculate the linear terms of the zeroth-order collision integrals
S_p	=	reaction velocity of the pth process
S_{rec}	=	three-body recombination source term for the Boltzmann equation
S_{sup}	=	superelastic collision source term for the Boltzmann equation
S_0	=	zeroth-order collision integrals
$\mathbf{S}_1$	=	first-order collision integrals
T	=	gas temperature
T_{Ar}	=	argon internal temperature
T_e	=	electron temperature

Presented as Paper 4126 at the 38th AIAA Plasmadynamics and Laser Conference, Miami, FL, 25–28 June 2007; received 16 July 2007; revision received 23 January 2008; accepted for publication 30 January 2008.

*Senior Researcher, Istituto di Metodologie Inorganiche e dei Plasmi, Sede di Bari, Via Amendola 122/D; gianpiero.colonna@ba.imip.cnr.it. Member AIAA.

†Full Professor, Dipartimento di Chimica; mario.capitelli@ba.imip.cnr.it. Member AIAA.

t = time
u = flow speed
V = electric potential
$\mathbf{v}$ = velocity vector
$\mathbf{v}_d$ = electron drift velocity
X, Y = reactants and products
x = position along the nozzle axis
x_a = position of the lower extreme of the electrodes
x_0 = nozzle inlet
α = over- and under-relaxation coefficient
α_p = constant pressure specific heat/ideal-gas constant
$\alpha^\star$ = upper limit for α
ϵ = electron energy
ε_{med} = electron mean energy
ϵ_{sv} = internal level energy
$\epsilon^\star$ = threshold energy of the considered transition
ν_e = electron-heavy-particle elastic collision frequency
ν_{sul} = emission frequency for the sth species in the $u \rightarrow l$ transition
ρ = mass density
σ_i = cross section of the ionization process
σ_r = cross section of the recombination process
φ_i = $\cos \vartheta_i$
ϑ_i = angle between a vector and the ith reference-frame axis
χ_s = molar fraction
$\hat{\Omega}$ = $\hat{\omega}^{-1}$
$\hat{\omega}$ = tensor inducing current anisotropy

Subscripts

k = index for internal iteration for nonlinear ordinary-differential-equation integration
p = reaction index
s = index for species
v = index for internal levels
0 = index for inlet values

I. Introduction

MANY efforts have been devoted to investigating the influence of a magnetic field on high-enthalpy flows [1–6], including recent experiments performed to study the behavior of a plasma jet impinging a sharp body immersed in a magnetic field [7–9]. The observed nonequilibrium ionization and the anomalous electron temperature, measured by spectroscopic or microwave absorption techniques, lead to the conclusion that non-Maxwell electron energy distribution functions are present in the system [7–9].

A self-consistent model that couples the state-to-state master equation for heavy-particle kinetics and the Boltzmann equation for free electrons in electric and magnetic fields has been investigated for an argon gas expanding through a converging–diverging nozzle in supersonic conditions [10], which do not take into account magnetohydrodynamic (MHD) interactions. Attention was focused on the influence of orthogonal electric and magnetic fields, the latter oriented in the same direction of the flow, in affecting the electron energy distributions in supersonic nozzle expansion. A competitive behavior of the electric and magnetic fields is observed, the latter tending to annihilate the effect of the former. A relevant contribution comes from argon metastable states that strongly influences the electron distributions through superelastic electronic collisions.

The solution of the Boltzmann equation determines the electron energy distribution function (EEDF) from which it is possible to calculate macroscopic electron transport coefficients such as the tensorial mobility [1–9] and global rates [10]. Nonequilibrium distributions induce special behaviors of such parameters, such as the departure from the Arrhenius trend of the rate coefficients of ionization or, in general, for electron-induced chemical processes [10–12]. Another limitation of the model in [10] is the constant-electric-field approximation, which, in some conditions, leads to an exponential growth of the electron density, limited only by full ionization.

In this work, we will apply the model described in [10] (also see the Appendix) for investigating supersonic nozzle expansion with field configurations in which a MHD interaction is effective. Moreover, the electron density growth was limited by simulating a polarization circuit with a resistor.

II. Numerical Model

The nozzle-expansion model consists of self-consistently coupling three different computational blocks: fluid dynamics, chemical and level kinetics, and the free-electron Boltzmann equation. The master role is played by the fluid dynamics code, which solves the Euler equations in quasi-1-D approximation [13]. This block also manages the external conditions such as the electric and magnetic fields. The previous code [10] was improved to account for MHD interaction (Faraday electromotive field) and to limit the plasma current induced by the external electric field.

The fluid dynamics block also determines the computational grid points using a step-adaptive algorithm to keep the truncation error of relevant quantities below a given tolerance (see [14]).

A. Fields

The electric field contributes to the energy equation

$$\frac{\mathrm{d}}{\mathrm{d}x}\left(\frac{1}{2}u^2 + h_T + h_{\text{in}}\right) = \frac{\dot{Q}}{\rho u} \tag{1}$$

by adding a Joule heating contribution [15,16]

$$\dot{Q}_J = \mathbf{J} \cdot \mathbf{E} = -eN_e \mathbf{v}_{\text{d}} \cdot \mathbf{E} \tag{2}$$

to $\dot{Q}$. The drift velocity is calculated directly from the electron energy distribution function, as described in the Sec. II.C. An additional contribution to $\dot{Q}$ comes from radiative losses:

$$\dot{Q}_{\text{rad}} = \sum_{s,u,l} \dot{A}_{sul} h \nu_{sul} N_{su} \tag{3}$$

This contribution was neglected in the present work, because we are considering only metastable states; it could become relevant if higher excited levels were considered.

An electric field applied to a gas can cause a rapid growing of the degree of ionization, limited only by the breakdown (full ionization). This phenomenon is intrinsically time-dependent and it hardly fits with a stationary step-marching algorithm, as was used for the nozzle flow calculation [13]. An approximate approach to limit the discharge current, as well as the ionization degree, was considered. The electric field is generated by parallel flat-plate electrodes connected with a power supply by a circuit with a resistor R_c. By Ohm's law,

$$V_{\text{discharge}} = V_{\text{generator}} - R_c I \tag{4}$$

where the current can be calculated in a 1-D approximation as

$$I(x) = \int_{x_a}^{x} \mathbf{J} \cdot \frac{\mathbf{d}}{|\mathbf{d}|} \frac{\mathrm{d}S_e}{\mathrm{d}t}\,\mathrm{d}t \tag{5}$$

and for parallel plates (neglecting the border effects),

$$\mathbf{E}(x) = V_{\text{discharge}} \frac{\mathbf{d}}{|\mathbf{d}|^2} = \mathbf{E}_{\text{generator}} - \frac{R_c \mathbf{d}}{|\mathbf{d}|^2} \int_{x_a}^{x} \mathbf{J} \cdot \frac{\mathbf{d}}{|\mathbf{d}|} \frac{\mathrm{d}S_e}{\mathrm{d}t}\,\mathrm{d}t \tag{6}$$

This equation is not correct, because the field is affected only locally and not in all of the regions between the electrodes. Moreover, the field calculated with Eq. (6) does not satisfy Maxwell equations, with $\nabla \wedge \mathbf{E}$ being different from zero. The correct approach should consider the derivative in the x direction of the y component of the field or, alternatively, an oscillating magnetic field. This is not feasible in the present model, which is 1-D and stationary. Nevertheless, if one wants to estimate the postdischarge conditions, Eq. (6) qualitatively reproduces the discharge behavior, reducing the

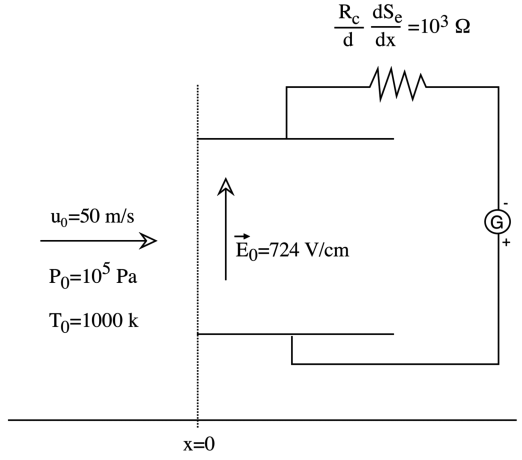

Fig. 1 Geometrical configuration and initial conditions for the uniform section case.

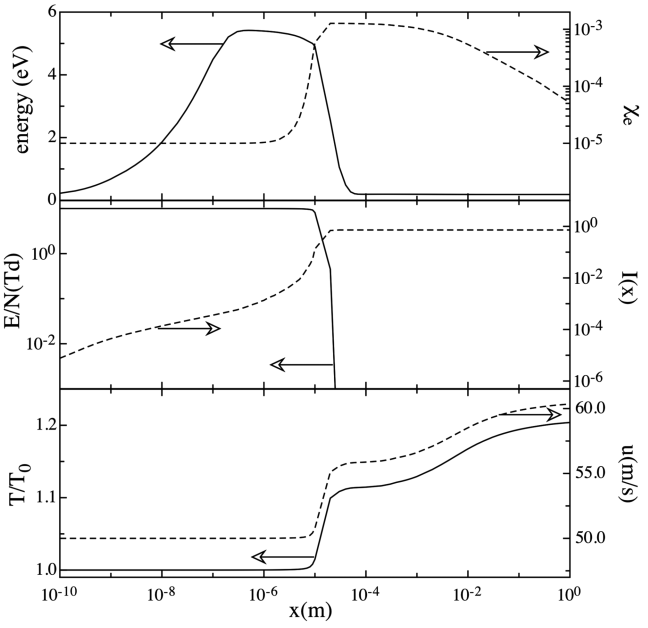

Fig. 2 Space profile of different quantities (electron mean energy and fraction, reduced electric field and current, gas temperature and flow speed) along the flow for the case reported in Fig. 1.

electric field and the ionization growth as the current increases, consistently with a space-marching algorithm. To test this model, a uniform duct section was considered. Geometry and initial conditions are described in Fig. 1, and relevant macroscopic quantities are reported in Fig. 2 as a function of the position along the nozzle axis.

We can observe three different regions: for $x < 10^{-5}$ m, the electric field first causes an abrupt increase of the electron energy (at constant ionization degree), followed by an increase of the degree of ionization (for constant electron mean energy). In that region, the current is still weak and the Joule heating has no effect. Between 10^{-5} and 2×10^{-5}, the electron density grows very fast, the current becomes high enough to reduce the electric field, and part of the electric work heats the gas and increases the flow speed. For $x > 2 \times 10^{-5}$, the electric field goes to zero and the electron temperature decreases. Electron–ion recombination becomes effective and the energy released goes into the gas temperature and speed. This behavior is reflected on the EEDF, as shown in Fig. 3. In the first region (left plot in Fig. 3), the EEDF is heated. When the electric field decays (right plot of Fig. 3), the distributions cool down and show typical peaks due to superelastic collisions and recombination. For $x > 2 \times 10^{-5}$, the effects due to superelastic

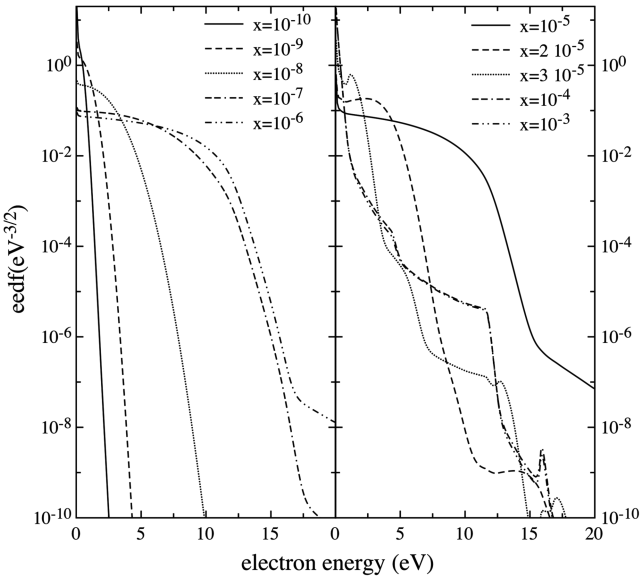

Fig. 3 Electron energy distributions in different positions in the same conditions as in Fig. 2.

collisions become more important in transferring energy from ions and metastable states to electrons (the plateaux increase) and from electrons to the gas to reproduce postdischarge conditions [17].

The magnetic field is responsible for two different contributions. The first contribution is the Faraday electromotive field

$$\mathbf{E}_{\mathrm{F}} = \mathbf{u} \wedge \mathbf{B} \tag{7}$$

which is equivalent to an electric field, and the second contribution is the force

$$\mathbf{F}_{\mathrm{MHD}} = \mathbf{J} \wedge \mathbf{B} = -eN_e\mathbf{v}_d \wedge \mathbf{B} \tag{8}$$

which must be added to the momentum equation:

$$\frac{\mathrm{d}P}{\mathrm{d}x} + \rho u \frac{\mathrm{d}u}{\mathrm{d}x} = F_x \tag{9}$$

B. Fluid Dynamics

Following the approach described in [13], Euler equations are rewritten as pseudoconservation equations:

$$\begin{cases} \rho u A = \mathcal{K}_m \\ AP + \mathcal{K}_m u = \mathcal{K}_P \\ \frac{u^2}{2} + \alpha_p R^\star T + h_{\mathrm{in}} = \mathcal{K}_e \end{cases} \tag{10}$$

where $\mathcal{K}$ pseudoconstants

$$\begin{cases} \mathcal{K}_m = \rho_0 u_0 A_0 \\ \mathcal{K}_P = A_0 P_0 + \mathcal{K}_m u_0 + \int_{x_0}^{x} \left(P(t)\frac{\mathrm{d}A(t)}{\mathrm{d}t} + AF_x(t)\right)\mathrm{d}t \\ \mathcal{K}_e = \frac{u_0^2}{2} + \alpha_{p0} R_0^\star T + h_{\mathrm{in},0} + \int_{x_0}^{x} \dot{Q}(t)\,\mathrm{d}t \end{cases} \tag{11}$$

These equations differ from those in [13] by introducing the force term F_x and the energy production rate $\dot{Q}$. Equations (10) and (11) are closed with the perfect-gas-state law and the definition of the internal energy from composition and level distribution:

$$h_{\mathrm{in}} = \frac{1}{\bar{m}} \sum_s \chi_s \left[H_s^f + \sum_{v=1}^{L_s} f_{sv}\epsilon_{sv} \right] \tag{12}$$

The numerical solution of Eq. (10) is obtained as described in [13].

C. Free Electrons

The free-electron kinetics are studied, solving the Boltzmann equation in the two-term approximation [10,15,16] (see the Appendix), which is valid for a weakly anisotropic distribution. Under this approximation, the Boltzmann equation for the electron energy distribution function can be written as

$$\frac{\partial n_0(\epsilon)}{\partial t} = -\frac{\partial J_{\rm el}(\epsilon)}{\partial \epsilon} - \frac{\partial J_f(\epsilon)}{\partial \epsilon} - \frac{\partial J_{\rm ee}(\epsilon)}{\partial \epsilon} - \frac{\partial J_{\rm ne}(\epsilon)}{\partial \epsilon} + S_{\rm in}(\epsilon) + S_{\rm sup}(\epsilon) + S_{\rm ion}(\epsilon) + S_{\rm rec}(\epsilon) \tag{13}$$

It should be noted that the Boltzmann equation contains flux J and source S terms. Explicit expressions for the J and S terms in the absence of a magnetic field can be found in [15,16,18]. The contribution of the magnetic field enters in the field flux term coupled with the electric field:

$$J_f = \frac{2e}{3m_e}\mathbf{E}\hat{\omega}(\mathbf{B})\mathbf{E}\sqrt{\epsilon^3}\frac{\partial}{\partial \epsilon}\left(\frac{n_0}{\sqrt{\epsilon}}\right) \tag{14}$$

where the tensor $\hat{\omega}$ is defined in the Appendix [see Eq. (A33)]. It can be shown that the scalar term $\mathbf{E}\hat{\omega}\mathbf{E}$ in Eq. (14) decreases as the magnetic field increases, thereby reducing the heating effect due to the applied electric field. This result, observed also in a previous work [10], is not valid if the Faraday electromotive field is considered.

Equation (13) refers only to the homogeneous part of the electron distribution. The anisotropic term, from which we can calculate the drift velocity [see Eq. (A50) in the Appendix], under the quasi-stationary approximation, can be obtained directly from the EEDF by

$$\mathbf{v}_d = \int_0^\infty \mathbf{n}_1 \, {\rm d}\epsilon \tag{15}$$

As a consequence of Eq. (15), the electron mobility has the same tensorial structure as the matrix $\hat{\omega}$. In this way, it is possible to consider the Hall current.

The term $J_{\rm ne}$ introduced in [10] is responsible for the electron distribution cooling due to the expansion of the electron gas. This term is an approximation of spatial gradients (see [10]) and reduces the electron energy to balance the increase of the flow velocity:

$$J_{\rm ne}(\epsilon) = \frac{m_e}{e}n_0(\epsilon)u\frac{\partial u}{\partial t} \tag{16}$$

This term allows one to couple the Boltzmann equation for free electrons [see Eq. (13)] with a stationary 1-D nozzle-expansion code in the same way as a master equation for internal levels, replacing the time derivative as the substantial derivative:

$$\frac{{\rm d}n_0(\epsilon)}{{\rm d}t} \to \frac{{\rm d}uAn_0(\epsilon)}{A\,{\rm d}x} \tag{17}$$

It must be also noted that the losses due to elastic collisions $J_{\rm el}$ are larger than those due to expansion.

The flux terms J take into account continuous energy exchange, and the source terms S_x consider jumps in the energy ladder, which are due to inelastic and superelastic collisions $S_{\rm in}$ and $S_{\rm sup}$, which induces internal energy transitions to chemical processes: in this case, ionization $S_{\rm ion}$ and three-body recombination $S_{\rm rec}$. The latter terms are similar to those of inelastic and superelastic collisions, respectively, but particular care must be taken to calculate the cross section of the recombination process through the detailed balance principle. Considering electron-induced ionization of Ar,

$$e(\epsilon) + {\rm Ar}(i) \rightleftharpoons e(\epsilon - \epsilon^\star) + {\rm Ar}^+(j) + e(0) \tag{18}$$

the detailed balance relates ionization i and recombination r cross sections with the following relation:

$$\sigma_r(\epsilon - \epsilon^\star) = F(\epsilon)G(T) \qquad F(\epsilon) = \frac{\epsilon}{\epsilon - \epsilon^\star}\sigma_i(\epsilon)\frac{g_i^{\rm Ar}}{g_j^{\rm Ar^+}}$$
$$G(T) = \frac{Q_{\rm Ar^+}(T)}{Q_{\rm Ar}(T)K_{\rm eq}(T)}\exp\left(-\frac{\epsilon^\star}{kT}\right) \tag{19}$$

which is different from the relation between the inelastic and the relative superelastic cross sections. The internal partition functions Q are calculated considering only the levels included in the simulation. This method assures that at equilibrium, the composition is the real equilibrium composition and the electron distribution is Maxwellian.

The source terms are strictly related to the master equation, depending on the composition and level distribution. Moreover, from cross sections and EEDF, the rate coefficients for the heavy-particle master equation are calculated as

$$R_p = \int_0^\infty \sigma(\epsilon)v(\epsilon)n_0(\epsilon)\,{\rm d}\epsilon \tag{20}$$

D. Chemical Kinetics

A reduced master equation for heavy-particle argon kinetics is considered, including ground Ar^0 and metastable $Ar^\star$ (with $\epsilon^\star = 11.55$ eV) states. We account for the excitation–deexcitation and ionization-recombination processes from ground and metastable argon, induced both by collisions with atoms and with electrons:

$$\begin{array}{ll} {\rm Ar}^0 + e \rightleftharpoons {\rm Ar}^\star + e & {\rm Ar}^0 + {\rm Ar}^0 \rightleftharpoons {\rm Ar}^\star + {\rm Ar}^0 \\ {\rm Ar}^0 + e \rightleftharpoons {\rm Ar}^+ + e + e & {\rm Ar}^0 + {\rm Ar}^0 \rightleftharpoons {\rm Ar}^+ + e + {\rm Ar}^0 \\ {\rm Ar}^\star + e \rightleftharpoons {\rm Ar}^+ + e + e & {\rm Ar}^\star + {\rm Ar}^0 \rightleftharpoons {\rm Ar}^+ + e + {\rm Ar}^0 \end{array}$$

In this kinetic model, we are neglecting the formation of excimer species (such as Ar_+^2 and $Ar_\star^2$), which can be important, especially at high pressure and low temperature (conditions not met in the nozzle expansion considered here). The master equation is strongly nonlinear, and each process adds a source term, such as

$$\sum_i c_{pi}^{\rm re}X_i \rightleftharpoons \sum_j c_{pj}^{\rm pr}Y_j \qquad S_p = R_p(T)\prod_i N_i^{c_{pi}^{\rm re}} \tag{21}$$

For the reactants, the contribution in the ith relaxation equation is $-c_{pi}^{\rm re}S_p$, whereas for products, it must be added: $+c_{pj}^{\rm pr}S_p$.

The solution to the system of equations uses a full nonlinear algorithm. It starts by calculating a kinetic matrix $\hat{M}$ to linearize the problem

$$\frac{{\rm d}N_i}{{\rm d}t} \approx \frac{N_i^k(t+\Delta t) - N_i(t)}{\Delta t} = \hat{M}(N_i^{k-1}(t+\Delta t))N_i^k(t+\Delta t)$$
$$(\hat{I} - \Delta t\hat{M}(N_i^{k-1}(t)))N_i^k(t+\Delta t) = N_i(t) \tag{22}$$

and to iterate the procedure in Eq. (22) until the variation is smaller than a given tolerance. The initial guess $N_i^0(t+\Delta t)$ can be determined in different ways. The simplest approach is to consider $N_i^0(t+\Delta t) = N_i(t)$. In the code, we can also consider the initial guess to be the extrapolation of the two previous time steps. To stabilize the algorithm, we consider an over- and under-relaxation procedure:

$$(\hat{I} - \Delta t\hat{M}(N_i^{k-1}(t+\Delta t)))N_i^\star = N_i(t)$$
$$N_i^k(t+\Delta t) = \alpha N_i^\star + (1-\alpha)N_i^{k-1}(t+\Delta t) \tag{23}$$

The coefficient α can vary between 0 and 2, and its value is changed to avoid numerical oscillations. To improve procedure convergence speed, α should be limited by a value lower than two, and it was fixed to 1.8. If the error (the difference between two successive approximations) is lower than the tolerance, α is increased, if it is larger than the error upper limit, it is decreased. Then the convergence is reached when the error is lower than the tolerance for the maximum possible α. In some cases, such a maximum value

cannot be reached because the algorithm is stable for $\alpha^\star$ but not for $\alpha^\star + \delta$. In this case, the convergence criterion must be fulfilled with $\alpha^\star$ even if it is smaller than its upper limit. This method was also applied in coupling heavy-particle and free-electron kinetics.

The previous algorithm is completed with a step-adaptive criterion [14]. This method evaluates the truncation error by comparing the new solution with the linear extrapolation of the two previous steps. The algorithm used here is very stable and fast. The previous discussion refers to the time evolution of an homogeneous system. To pass to the species continuity equation, we must substitute the time derivative as in Eq. (17), converting particle densities to mass densities.

III. Results

The preceding model was applied to two different test cases. In the first case study, we report the effect of an electric field applied at the nozzle inlet on the relevant quantities at the nozzle exit. In the second case, we report the interplay of the electric and magnetic fields, including the electromotive force, on the thermochemistry and fluid dynamics along the nozzle axis.

A. Electric Field

The studied system is shown in Fig. 4 (see [8,9]). The nozzle inlet is at $x = -0.1$ m and the exit is at $x = 0.28$ m with respect to the throat. Inlet pressure and temperature were, respectively, at 1 atm and at 1000 K, and the inlet ionization degree was set at 10^{-5}. As in Figs. 2 and 3, $R_{cr} = 10^3$ is kept constant. The electrode dimension was considered small (10^{-5} m) to reduce computational time.

The flow properties were investigated for different values of the reduced electric field E/N ranging from 10 to 40 Td. Increasing the electric field causes the energy density of the system to increase, due to the contribution in the Euler equations [see Eq. (1)] of the Joule source term given in Eq. (2).

On the other hand, the Mach number, slightly growing for low electric fields, decreases for $E/N > 20$ Td (see Fig. 5). For $E/N < 20$ Td, most of the work done by the field is transferred to the translational degrees of freedom of the gas, acting on the temperature and the flow speed. For $E/N > 20$ Td, most of the energy supplied by the electric field promotes electron impact ionization. Moreover, one should consider that by increasing the ionization degree, the gas density decreases.

At intermediate field strength (approximately 15 Td), a small minimum is present in Fig. 5. This is due to the relevant contribution of inelastic collisions, which transfer energy to internal levels. These effects can be observed in Fig. 6, in which we have plotted gas temperature, electron, and Ar metastable molar-fraction profiles. The increase of the gas temperature is not proportional to the increase of total energy density; but the ratio between temperature and total energy density reduces by a factor of 2, changing from 10 to 40 Td. As described in the previous section, the electron molar fraction sharply increases as a function of E/N. The electron molar fraction is almost constant along the nozzle (also see [8,9]), but when the applied field vanishes, a slight decrease of the electron density is observed. For high applied field strength (greater than 30 Td), the degree of ionization is very high (approximately 0.1). In these cases, the electron gas does not cool down efficiently, because this process is dominated by electron–ion coulomb collisions; consequently, the recombination is slow for the high electron mean energy, as can be observed in Fig. 6.

The metastable kinetic behavior is strongly coupled to the electron density. For a low electron molar fraction (corresponding to fields $E/N < 30$ Td), the metastable-state concentration follows the electron density in the converging part of the nozzle, whereas in the outlet, its population decreases due to the superelastic collisions. On the other hand, for high electric fields (greater than 30 Td), the population of the metastable state increases after the throat, due to dominance of electron–ion recombination with respect to superelastic collisions.

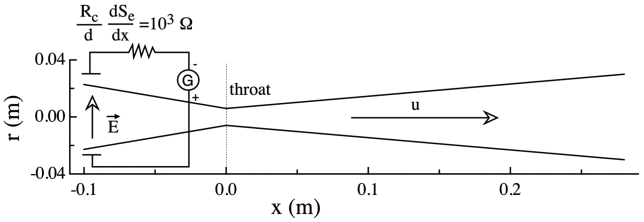

Fig. 4 Nozzle profile and external circuit.

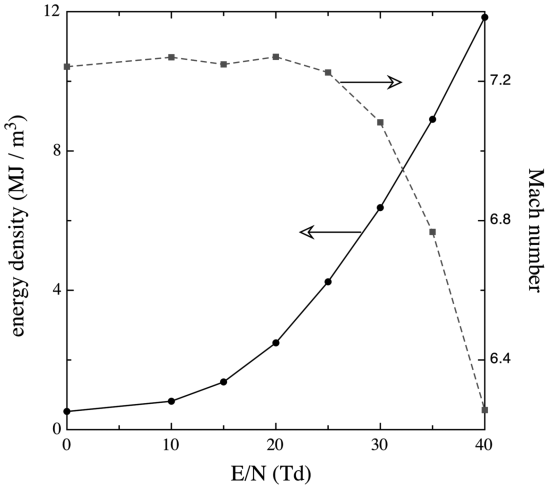

Fig. 5 Energy density and Mach number at the nozzle exit as a function of the reduced unperturbed electric field.

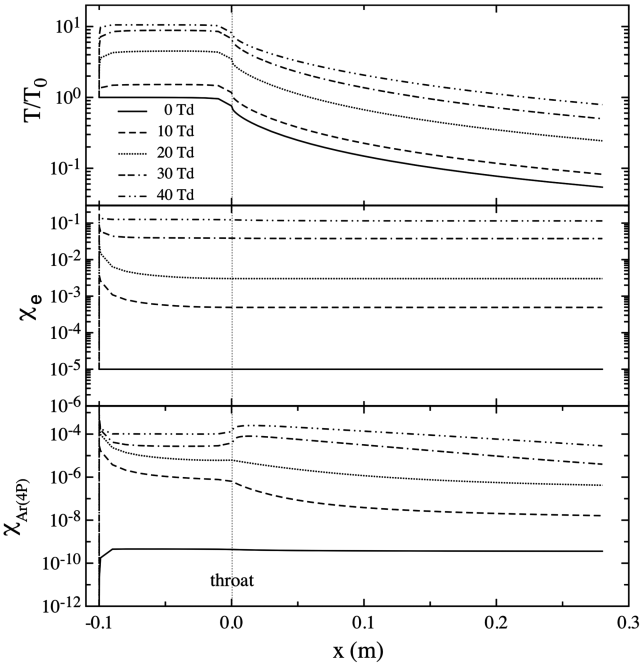

Fig. 6 Gas temperature, electron and metastable argon molar-fraction profiles for different applied electric field.

The EEDF profiles (see Fig. 7) closely follow the corresponding temperature and molar-fraction profiles. Inspection of this figure shows that in the nozzle throat, the EEDF profiles for $E/N < 30$ Td present the typical plateaux and peaks due to superelastic collisions, whereas for $E/N > 30$ Td, the EEDF becomes nearly Maxwellian, due to the thermalization of electron–electron coulomb collisions. It should be also noted that the synergic contribution of electron–electron and superelastic collisions keeps the electron temperature

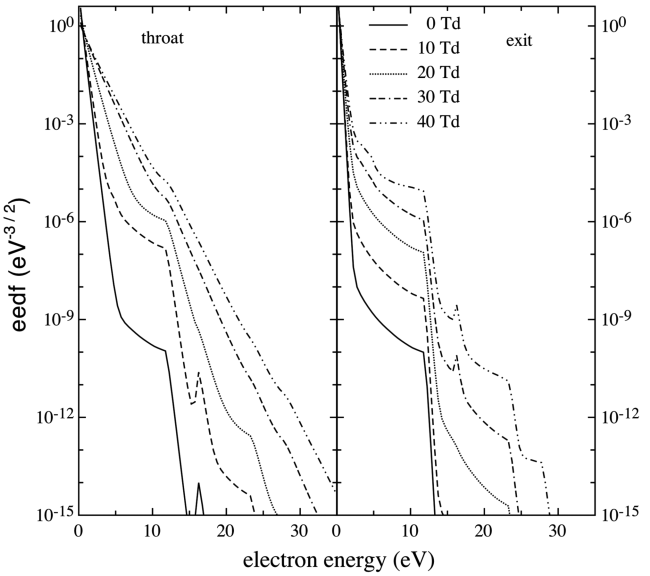

Fig. 7 Throat and exit electron energy distributions for different electric fields.

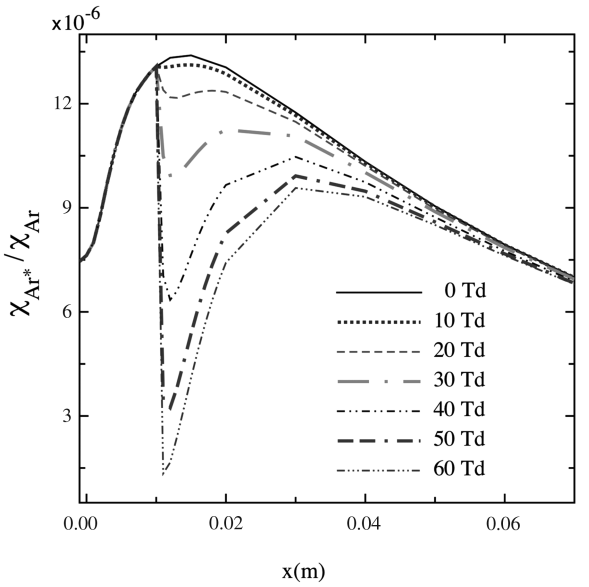

Fig. 8 Population profile of Ar metastable state as a function of the applied electric field.

higher than the gas temperature. At the nozzle exit, elastic collisions are capable of cooling the distribution, emphasizing the formation of plateaus due to the superelastic collisions.

It is interesting to show the situation created by applying the electric field in the expansion region in which the flow is supersonic. In this case, the inlet conditions, roughly reproducing the postdischarge conditions previously obtained for $E/N = 20$ Td, are as follows:

$$P_0 = 1 \text{ bar} \qquad T_0 = 7000 \text{ K} \qquad T_e = 10,000 \text{ K}$$
$$T_{\text{Ar}} = 10,000\ K \qquad \chi_e = 10^{-2}$$

The external electric field, for which the amplitude is varied up to 60 Td, is applied in the y direction between $x = 0.01$ and 0.02 m, and the speed is around Mach 2. The influence on the flow properties is very weak because, due to the high ionization degree, the current increases in a very small space interval, limiting the effects of the electric fields. On the contrary, the population of metastable states is strongly influenced by the applied electric field, as can be observed in Fig. 8. As soon as the electric field is on, the population of the metastable $\text{Ar}^\star$ decreases, due to electron impact ionization of excited argon. When the electric field vanishes, the three-body recombination process repopulates the metastable state independently of the applied field. This result can be useful for the spectroscopic characterization of flows. Applying an electric field to a plasma undergoing a supersonic expansion, it is possible to enhance the radiation emission in a selected position, minimizing interferences with flow conditions and gas composition.

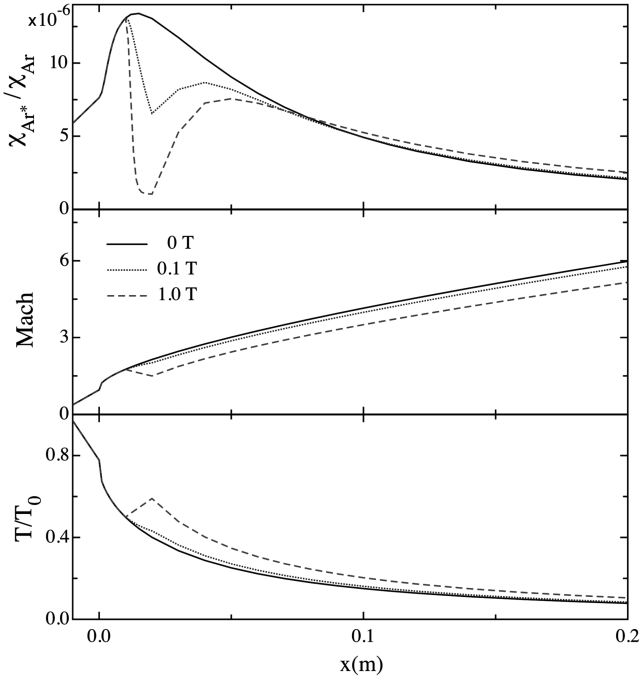

Fig. 9 Metastable Ar, Mach, and gas temperature profiles for different magnetic fields with no electric field.

B. Magnetic Field

To study the effects of the magnetic field on high-enthalpy flow, the same nozzle as in the previous section was considered with the initial conditions listed in the previous section. As a first example, only the magnetic field (up to 1 T) is applied in the region of 0.01–0.02 m. In this case, the contribution of the Faraday field (7) and MHD interaction (8) are considered.

The Faraday field produces results that are similar to a real electric field. Different from an external electric field, the current produced by the Faraday electromotive force is not limited. As a consequence, the effect on macroscopic properties is stronger. It must also be considered that, due to the MHD interaction, the magnetic field strongly affects macroscopic quantities, contrary to the electric field, not only in the field region, but also at the nozzle exit, as can be observed in Fig. 9.

Let us now consider the case in which electric and magnetic fields are simultaneously applied. The electric and magnetic fields lie, respectively, in the y and z directions, and so $\mathbf{E} \wedge \mathbf{B}$ is oriented in the positive x direction. The magnetic field, in the absence of the electric field, can induce appreciable changes in the Mach number (up to 15%) and temperature (up to 30%) at the nozzle exit (see Fig. 10). Moreover, for $B < 0.1$ T, the electric and magnetic fields have synergic effects, whereas for $B = 1$ T, they compensate each other.

The electron energy distribution functions at $x = 0.02$ m, where the fields are practically vanishing, are plotted in Fig. 11. When only the magnetic field is applied (left plot), increasing the field will increase the electron distribution for $\epsilon < 12$ eV, until the plateau produced by superelastic collisions is hidden (see the $B = 1$ T case.)

When a 60-Td electric field is applied in the same region, a nonmonotonic dependence of the EEDF on the B field is observed

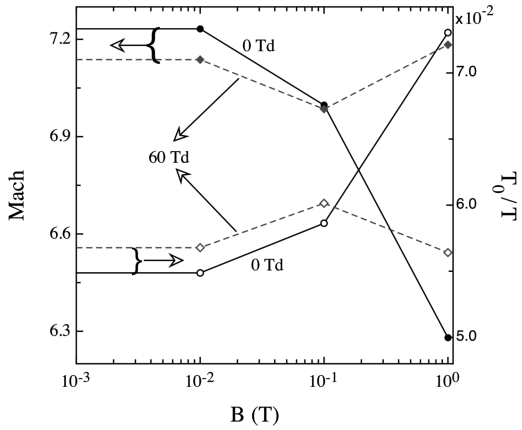

Fig. 10 Mach and temperature at the nozzle exit for different applied electric and magnetic fields.

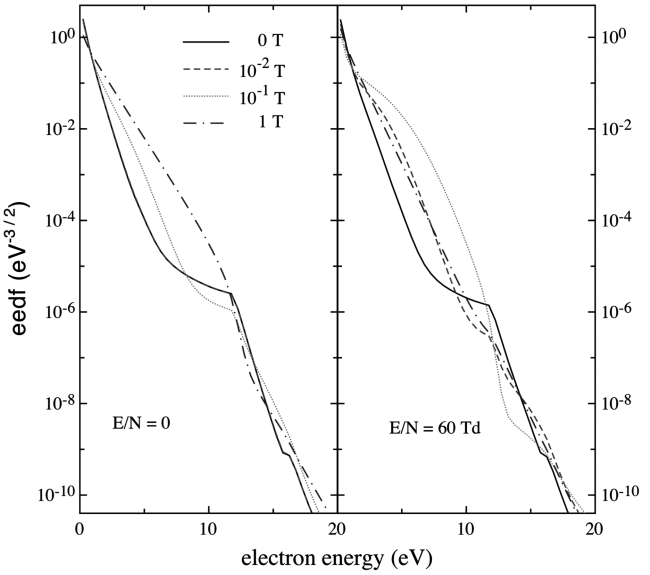

Fig. 11 Electron energy distributions at $x = 0.02$ m (upper limit of the E and B field regions) for different magnetic field magnitude; comparison between $E/N = 0$ and 60 Td.

(see the right side of Fig. 11). It should be noted that the applied electric field is such that it removes the quasi coincidence of the EEDF for a magnetic field value $\leq 10^{-2}$ T observed at $E/N = 0$.

IV. Conclusions

We presented a model to study MHD interactions based on the self-consistent coupling of electronically excited state kinetics, the Boltzmann equation for free electrons, and the Euler equations for flow. Electrical and magnetic fields were included in both the kinetic and fluid dynamics equations. Macroscopic parameters of the plasma (conductivity, ionization, and excitation rates) are strongly influenced by the electron energy distributions, and departure from a Maxwellian distribution can induce special behavior of such quantities. The effects of electric and magnetic fields on a supersonic nozzle expansion were investigated by considering different field configurations. The model predicts nonequilibrium inlet conditions for arc-heated argon jets, also observed in some experiments [7–9]. We also investigated the possibility of using electric and magnetic fields in supersonic expanding plasma to modify the flowfield or for enhancing optical emission. Also in this case, nonequilibrium plays a fundamental role in the determination of the plasma properties.

The extension of this model to more complex systems such as molecular gases (N_2 or O_2) or mixtures (air), including state-to-state vibrational kinetics, is in progress in this laboratory.

Appendix: Boltzmann Equation in Two-Term Approximation

The general form of the Boltzmann equation,

$$\frac{\partial f(\mathbf{r},\mathbf{v},t)}{\partial t} + \mathbf{v}\cdot\nabla_r f(\mathbf{r},\mathbf{v},t) + \mathbf{a}\cdot\nabla_v f(\mathbf{r},\mathbf{v},t) = \left(\frac{\delta f}{\delta t}\right)_{\text{coll}} \tag{A1}$$

describes the time evolution of the distribution function f of a species: in this case, electrons in phase space. The term $(\delta f/\delta t)_{\text{coll}}$ is the Boltzmann collision integral. The numerical integration of the Boltzmann equation is not possible due to the large number of degrees of freedom. For free electrons in weakly ionized gases and for small electric fields, the two-term approximation is commonly used.

I. Two-Term Approximation

This approximation consists of assuming that the electron distribution is almost isotropic and truncating (to the first order) the expansion in spherical harmonics, to give

$$f(\mathbf{r},\mathbf{v},t) = f_0(\mathbf{r},v,t) + \frac{\mathbf{v}}{v}\cdot\mathbf{f}_1(\mathbf{r},v,t) \tag{A2}$$

Considering the angle variables

$$\varphi_i = \frac{v_i}{v} = \cos\vartheta_i \tag{A3}$$

the integrals in the velocity space can be transformed as

$$-\iiint_{\infty}^{\infty} \mathrm{d}^3v = \frac{\pi}{2}\int_0^{\infty} v^2\,\mathrm{d}v \iiint_{-1}^{1} \mathrm{d}^3\varphi \tag{A4}$$

The integrals over the φ variables are of the kind

$$\int_{-1}^{1} \varphi_i^{q-1}\,\mathrm{d}\varphi_i = 2\frac{a|2}{a} \tag{A5}$$

where the symbol $a|2$ is the modulus function (zero for even numbers and one for odd numbers). The isotropic f_0 and anisotropic $\mathbf{f}_1$ parts of the distribution can be obtained as

$$f_0(\mathbf{r},v,t) = \frac{1}{8}\iiint_{-1}^{1} f(\mathbf{r},\mathbf{v},t)\,\mathrm{d}^3\varphi \tag{A6}$$

$$\mathbf{f}_1(\mathbf{r},v,t) = \frac{3}{8}\iiint_{-1}^{1} \boldsymbol{\varphi} f(\mathbf{r},\mathbf{v},t)\,\mathrm{d}^3\varphi \tag{A7}$$

The first three moments of the distribution (particle density, mean velocity, and mean energy in electron volts) in the two-term approximation are calculated as

$$N_e = \iiint_v f(\mathbf{r},\mathbf{v},t)\,\mathrm{d}^3v = 4\pi\int_0^{\infty} v^2 f_0(\mathbf{r},v,t)\,\mathrm{d}v \tag{A8}$$

$$\mathbf{v}_d = \frac{1}{N_e}\iiint_v \mathbf{v} f(\mathbf{r},\mathbf{v},t)\,\mathrm{d}^3v = \frac{4\pi}{3N_e}\int_0^{\infty} v^3\mathbf{f}_1(\mathbf{r},v,t)\,\mathrm{d}v \tag{A9}$$

$$\varepsilon_{\text{med}} = \frac{m_e}{2eN_e}\iiint_v v^2 f(\mathbf{r},\mathbf{v},t)\,\mathrm{d}^3v = \frac{4\pi m_e}{eN_e}\int_0^{\infty} v^4 f_0(\mathbf{r},v,t)\,\mathrm{d}v \tag{A10}$$

It should be noted that the scalar properties (such as density and mean energy) are obtained from f_0, whereas the vectorial properties (such as the mean velocity) are calculated from $\mathbf{f}_1$.

II. Differential Equations

For free electrons in magnetized plasma, the acceleration a in Eq. (A1) is given by

$$\mathbf{a} = \mathbf{A} + \mathbf{v} \wedge \mathbf{R} \tag{A11}$$

where

$$\mathbf{A} = -\frac{e}{m_e}\mathbf{E} + \mathbf{g} \tag{A12}$$

$$\mathbf{R} = -\frac{e}{m_e}\mathbf{B} \tag{A13}$$

where the gravity acceleration g is usually negligible in weakly ionized gas applications.

The velocity gradient of the distribution is given by

$$\boldsymbol{\nabla}_v f = \frac{\mathbf{v}}{v}\frac{\partial f_0}{\partial v} + \frac{\mathbf{f}_1}{v} + \frac{\mathbf{v}}{v}\mathbf{v}\cdot\frac{\partial}{\partial v}\frac{\mathbf{f}_1}{v} = \boldsymbol{\varphi}\frac{\partial f_0}{\partial v} + \frac{\mathbf{f}_1}{v} + \boldsymbol{\varphi} v \boldsymbol{\varphi}\cdot\frac{\partial}{\partial v}\frac{\mathbf{f}_1}{v} \tag{A14}$$

Integrating all of the terms in Eq. (A1) over the φ variables and then substituting Eq. (A2), we have the following integrals:

$$\iiint_{-1}^{1}\frac{\partial f}{\partial t}\,\mathrm{d}^3\varphi = 8\frac{\partial f_0}{\partial t} \tag{A15}$$

$$\iiint_{-1}^{1}\mathbf{v}\cdot\boldsymbol{\nabla}_r f\,\mathrm{d}^3\varphi = \frac{8v}{3}\boldsymbol{\nabla}_r\cdot\mathbf{f}_1 \tag{A16}$$

$$\iiint_{-1}^{1}\mathbf{A}\cdot\boldsymbol{\nabla}_v f\,\mathrm{d}^3\varphi = \mathbf{A}\cdot\left(8\frac{\mathbf{f}_1}{v} + \frac{8v}{3}\frac{\partial}{\partial v}\frac{\mathbf{f}_1}{v}\right) = \frac{8\mathbf{A}}{3v^2}\cdot\frac{\partial v^2\mathbf{f}_1}{\partial v} \tag{A17}$$

$$\iiint_{-1}^{1}\mathbf{v}\wedge\mathbf{R}\cdot\boldsymbol{\nabla}_v f\,\mathrm{d}^3\varphi = 0 \tag{A18}$$

$$S_0 = \frac{1}{8}\iiint_{-1}^{1}\left(\frac{\delta f}{\delta t}\right)_{\mathrm{coll}}\mathrm{d}^3\varphi \tag{A19}$$

The calculation of S_0 is described in detail in [15,16,18].

For the anisotropic part, we can integrate the Boltzmann equation multiplied by $\boldsymbol{\varphi}$

$$\iiint_{-1}^{1}\boldsymbol{\varphi}\frac{\partial f}{\partial t}\,\mathrm{d}^3\varphi = \frac{8}{3}\frac{\partial\mathbf{f}_1}{\partial t} \tag{A20}$$

$$\iiint_{-1}^{1}\boldsymbol{\varphi}\mathbf{v}\cdot\boldsymbol{\nabla}_r f\,\mathrm{d}^3\varphi = \frac{8}{3}v\boldsymbol{\nabla}_r f_0 \tag{A21}$$

$$\iiint_{-1}^{1}\boldsymbol{\varphi}\mathbf{A}\cdot\boldsymbol{\nabla}_v f\,\mathrm{d}^3\varphi = \frac{8}{3}\mathbf{A}\frac{\partial f_0}{\partial v} \tag{A22}$$

$$\iiint_{-1}^{1}\boldsymbol{\varphi}\mathbf{v}\wedge\mathbf{R}\cdot\boldsymbol{\nabla}_v f\,\mathrm{d}^3\varphi = \frac{8}{3}\mathbf{R}\wedge\mathbf{f}_1 \tag{A23}$$

$$\mathbf{S}_1 = \frac{3}{8}\iiint_{-1}^{1}\boldsymbol{\varphi}\left(\frac{\delta f}{\delta t}\right)_{\mathrm{coll}}\mathrm{d}^3\varphi \tag{A24}$$

Combining these terms, we have the system of equations

$$\begin{cases}\frac{\partial f_0}{\partial t} + \frac{v}{3}\boldsymbol{\nabla}_r\cdot\mathbf{f}_1 + \frac{\mathbf{A}}{3v^2}\cdot\frac{\partial v^2\mathbf{f}_1}{\partial v} = S_0\\ \frac{\partial\mathbf{f}_1}{\partial t} + v\boldsymbol{\nabla}_r f_0 + \mathbf{A}\frac{\partial f_0}{\partial v} + \mathbf{R}\wedge\mathbf{f}_1 = \mathbf{S}_1\end{cases} \tag{A25}$$

The expression for $\mathbf{S}_1$ was derived in [15,16,18]:

$$\mathbf{S}_1 = -\nu_e\mathbf{f}_1 \tag{A26}$$

Other processes such as inelastic, superelastic, and electron–electron collisions must be taken into account in the collision frequency (see [15]), but their contribution is usually negligible.

From basic vector algebra, it is known that the vector product can be written in matrix form as

$$\mathbf{a}\wedge\mathbf{b} = \begin{pmatrix}0 & -a_z & a_y\\ a_z & 0 & -a_x\\ -a_y & a_x & 0\end{pmatrix}\begin{pmatrix}b_x\\ b_y\\ b_z\end{pmatrix} \tag{A27}$$

obtaining

$$\mathbf{R}\wedge\mathbf{f}_1 + \nu_e\mathbf{f}_1 = \begin{pmatrix}\nu_e & -\mathcal{R}_z & \mathcal{R}_y\\ \mathcal{R}_z & \nu_e & -\mathcal{R}_x\\ -\mathcal{R}_y & \mathcal{R}_x & \nu_e\end{pmatrix}\begin{pmatrix}f_{1x}\\ f_{1y}\\ f_{1z}\end{pmatrix} = \hat{\Omega}\mathbf{f}_1 \tag{A28}$$

Moreover, the quantity

$$\mathbf{Q}_0 = -\left(v\boldsymbol{\nabla}_r f_0 + \mathbf{A}\frac{\partial f_0}{\partial v}\right) \tag{A29}$$

depends only on the isotropic distribution. In this way, Eq. (A25) can be rewritten as

$$\begin{cases}\frac{\partial f_0}{\partial t} + \frac{v}{3}\boldsymbol{\nabla}_r\cdot\mathbf{f}_1 + \frac{\mathbf{A}}{3v^2}\cdot\frac{\partial v^2\mathbf{f}_1}{\partial v} = S_0\\ \frac{\partial\mathbf{f}_1}{\partial t} + \hat{\Omega}\mathbf{f}_1 = \mathbf{Q}_0\end{cases} \tag{A30}$$

where $\hat{\Omega}\mathbf{f}_1$ is a dissipation term, and $\mathbf{Q}_0$ is the driving force for the anisotropic part of the distribution.

III. Quasi-Stationary Approximation

Except in cases in which high-frequency electric fields are applied, the anisotropic part of the distribution relaxes more rapidly than the isotropic part. In this case, the quasi-stationary approximation $(\partial\mathbf{f}_1/\partial t) \approx 0$ can be used, and the anisotropic part of the distribution can be calculated by solving the algebraic equation

$$\hat{\Omega}\mathbf{f}_1 = \mathbf{Q_0} \tag{A31}$$

This equation can be easily solved to obtain

$$\mathbf{f}_1 = \hat{\Omega}^{-1}\mathbf{Q}_0 = \hat{\omega}\mathbf{Q}_0 \tag{A32}$$

where

$$\hat{\omega} = \frac{1}{\nu_e(\nu_e^2 + \mathcal{R}^2)}\begin{pmatrix}\nu_e^2 + \mathcal{R}_x^2 & \mathcal{R}_x\mathcal{R}_y + \nu_e\mathcal{R}_z & \mathcal{R}_x\mathcal{R}_z - \nu_e\mathcal{R}_y\\ \mathcal{R}_x\mathcal{R}_y - \nu_e\mathcal{R}_z & \nu_e^2 + \mathcal{R}_y^2 & \mathcal{R}_y\mathcal{R}_z + \nu_e\mathcal{R}_x\\ \mathcal{R}_x\mathcal{R}_z + \nu_e\mathcal{R}_y & \mathcal{R}_y\mathcal{R}_z - \nu_e\mathcal{R}_x & \nu_e^2 + \mathcal{R}_z^2\end{pmatrix} \tag{A33}$$

Substituting Eq. (A32) into the equation for f_0, we have

$$\frac{\partial f_0}{\partial t} + \frac{v}{3}\boldsymbol{\nabla}_r\cdot\hat{\omega}\mathbf{Q}_0 + \frac{\mathbf{A}}{3v^2}\cdot\frac{\partial v^2\hat{\omega}\mathbf{Q}_0}{\partial v} = S_0 \tag{A34}$$

For homogeneous systems, all of the space gradients vanish, obtaining

$$\frac{\partial f_0}{\partial t} - \frac{1}{3v^2}\frac{\partial}{\partial v}\mathbf{A}\cdot\hat{\omega}\mathbf{A}v^2\frac{\partial f_0}{\partial v} = S_0 \tag{A35}$$

IV. Electrons in Flow

The equations reported in the previous section were obtained by considering the gas to be at rest. For the case of a flowing gas, the electron transport equation should be modified. To determine the corrections due to the flowing gas, we must find the transform relation between inertial systems. We can suppose that Eqs. (A34) and (A35) are valid in a reference frame that moves and that the flow has velocity $\mathbf{u}$. The particle velocity in this new frame (v') is related to the velocity in the laboratory system (v) by $\mathbf{v}' = \mathbf{v} - \mathbf{u}$. The distribution function in this system is given by

$$f'(\mathbf{v}') = f(\mathbf{v}) = f_0(\mathbf{v}' + \mathbf{u}) + \frac{\mathbf{v}' + \mathbf{u}}{|\mathbf{v}' + \mathbf{u}|}\cdot\mathbf{f}_1(\mathbf{v}' + \mathbf{u}) \tag{A36}$$

Assuming that the flow speed is much lower than the thermal velocity ($\mathbf{v}' \approx \mathbf{v}$), we can expand the terms in Eq. (A36) in a Taylor series truncated to the first order:

$$\begin{aligned} &f_0(\mathbf{v}' + \mathbf{u}) \approx f_0(v') + \mathbf{u}\cdot\boldsymbol{\varphi}'\frac{\partial f_0(v')}{\partial v} \qquad \frac{\mathbf{v}' + \mathbf{u}}{|\mathbf{v}' + \mathbf{u}|} \approx \boldsymbol{\varphi}' \\ &\mathbf{f}_1(\mathbf{v}' + \mathbf{u}) \approx \mathbf{f}_1(v') + \mathbf{u}\cdot\boldsymbol{\varphi}'\frac{\partial \mathbf{f}_1(v')}{\partial v} \end{aligned} \tag{A37}$$

And applying the definition of f_0 and $\mathbf{f}_1$, we have

$$\begin{aligned} f_0'(v') &= \iiint_{-1}^{1} f'(\mathbf{v}')\,\mathrm{d}^3\varphi' = f_0(v) + \frac{1}{3}\mathbf{u}\cdot\frac{\partial \mathbf{f}_1(v)}{\partial v} \\ \mathbf{f}_1'(v') &= \iiint_{-1}^{1} \boldsymbol{\varphi}' f'(\mathbf{v}')\,\mathrm{d}^3\varphi' = \mathbf{f}_1(v) + \mathbf{u}\frac{\partial f_0(v)}{\partial v} \end{aligned} \tag{A38}$$

These transformation equations can be used to determine the corrections to the Boltzmann equation for a flowing gas. It must be pointed out that Eq. (A24) for $\mathbf{S}_1$ is valid in the reference frame in which the gas is at rest; therefore,

$$\mathbf{S}_1 = -\nu_e\mathbf{f}_1' = -\nu_e\mathbf{u}\frac{\partial f_0(v)}{\partial v} - \nu_e\mathbf{f}_1 \tag{A39}$$

from which it follows that Eq. (A34) is still valid if $\mathbf{Q}_0$ has the form

$$\mathbf{Q}_0 = -\left[v\nabla_r f_0 + (\mathbf{A} + \nu_e\mathbf{u})\frac{\partial f_0}{\partial v}\right] \tag{A40}$$

and Eq. (A35) becomes

$$\frac{\partial f_0}{\partial t} - \frac{1}{3v^2}\frac{\partial}{\partial v}\mathbf{A}\cdot\hat{\omega}(\mathbf{A} + \nu_e\mathbf{u})v^2\frac{\partial f_0}{\partial v} = S_0 \tag{A41}$$

It should also be noted that the term S_0 must be calculated considering $f'(\mathbf{v}')$. Neglecting electron–electron collisions, the collision integral is a linear function of the isotropic distribution:

$$\begin{aligned} S_0 = \hat{S}_{\mathrm{LC}}[f_0'(v')] &= \hat{S}_{\mathrm{LC}}\left[f_0(v) + \frac{1}{3}\mathbf{u}\cdot\frac{\partial \mathbf{f}_1(v)}{\partial v}\right] \\ &= \hat{S}_{\mathrm{LC}}\left[f_0(v) + \frac{1}{3}\mathbf{u}\cdot\frac{\partial\hat{\omega}\mathbf{Q}_0}{\partial v}\right] \end{aligned} \tag{A42}$$

A similar approach can be used to calculate the contribution of electron–electron collisions to $\mathbf{S}_1$ [15], considering the transformation in a reference frame that moves with the electron current ($\mathbf{f}_1' = \mathbf{0}$). However, the contribution of the flow to the collision integrals S_0 and S_1 is a second-order correction.

To couple electron kinetics with a fluid dynamics model, it is necessary to determine the interaction between the two fluids. Essentially, the two systems exchange, between each other, both energy and momentum. The energy balance is already considered in S_0, providing that one includes the corresponding terms in the fluid dynamics equations. On the other hand, the momentum exchange is usually neglected. To estimate the momentum exchange between electrons and heavy particles, we can start from the relaxation equation in the absence of fields and gradients,

$$\frac{\partial \mathbf{f}_1}{\partial t} = -\nu_e\mathbf{u}\frac{\partial f_0}{\partial v} - \nu_e\mathbf{f}_1 \tag{A43}$$

obtaining the macroscopic source of free-electron momentum due to drag from heavy particles:

$$\begin{aligned} \left(\frac{\partial \rho_e\mathbf{u}_e}{\partial t}\right)_{\mathrm{drag}} &= N_e m_e\frac{\partial \mathbf{v}_{vv}}{\partial t} = \frac{4\pi m_e}{3}\int_0^\infty v^3\frac{\partial \mathbf{f}_1}{\partial t}\,\mathrm{d}v \\ &= -\frac{4\pi m_e}{3}\int_0^\infty v^3\nu_e\left(\mathbf{u}\frac{\partial f_0}{\partial v} + \mathbf{f}_1\right)\mathrm{d}v \end{aligned} \tag{A44}$$

V. Electron Energy Distribution

The two-term Boltzmann equation is usually written for the electron energy distribution, defined as

$$n_0(\epsilon) = 4\pi\sqrt{\frac{2e^3\epsilon}{m_e^3}}f_0(v) \tag{A45}$$

$$\mathbf{n}_1(\epsilon) = \frac{8\pi\epsilon e^2\epsilon}{3m_e^2}\mathbf{f}_1(v) \tag{A46}$$

where

$$\epsilon = \frac{m_e}{2e}v^2$$

is the electron energy in electron volts. This change of variable transforms the velocity derivative and differential as

$$\frac{\partial}{\partial v} = \sqrt{\frac{2m_e\epsilon}{e}}\frac{\partial}{\partial\epsilon} \tag{A47}$$

$$\mathrm{d}v = \sqrt{\frac{e}{2m_e\epsilon}}\,\mathrm{d}\epsilon \tag{A48}$$

transforming Eqs. (A8) and (A9) as

$$N_e = \int_0^\infty n_0(\epsilon)\,\mathrm{d}\epsilon \tag{A49}$$

$$\mathbf{v}_{\mathrm{d}} = \int_0^\infty \mathbf{n}_1(\epsilon)\,\mathrm{d}\epsilon \tag{A50}$$

The resulting differential equations (A25) become

$$\begin{cases} \frac{\partial n_0}{\partial t} + \nabla_r\cdot\mathbf{n}_1 + \frac{m_e\mathbf{A}}{e}\cdot\frac{\partial \mathbf{n}_1}{\partial\epsilon} = S_0 \\ \frac{\partial \mathbf{n}_1}{\partial t} + \frac{2e\epsilon}{3m_e}\nabla_r n_0 + \frac{2\epsilon}{3}(\mathbf{A} + \nu_e\mathbf{u})\left(\frac{\partial n_0}{\partial\epsilon} - \frac{n_0}{2\epsilon}\right) + \hat{\Omega}\mathbf{n}_1 = \mathbf{0} \end{cases} \tag{A51}$$

and in quasi-stationary approximation, we have

$$\mathbf{n}_1 = -\frac{2e\epsilon}{3m_e}\hat{\omega}\left[\nabla_r n_0 + \frac{m_e}{e}(\mathbf{A} + \nu_e\mathbf{u})\left(\frac{\partial n_0}{\partial\epsilon} - \frac{n_0}{2\epsilon}\right)\right] \tag{A52}$$

VI. Electron Kinetics in Nozzle Flow

To obtain the two-term approximation of the Boltzmann equation for quasi-1-D nozzle flow, analogous to Euler equations, the space gradients must be substituted with

$$\nabla_r f \equiv \begin{pmatrix} \frac{1}{A}\frac{\partial A f}{\partial x} \\ 0 \\ 0 \end{pmatrix}$$

which makes the Boltzmann equation very complex, containing mixed derivatives in space and energy. Moreover, it was observed that during the expansion, the electron distributions cool down, mainly due to collisions, and therefore the approximate approach described by Eqs. (16) and (17) is adequate.

It can be easily verified that the mean electron energy variation corresponds to the electron kinematic energy variation. In fact,

$$\delta\varepsilon_{\text{med}} = \delta\int_0^\infty \epsilon n_0(\epsilon)\,\mathrm{d}\epsilon = \int_0^\infty \epsilon\delta n_0(\epsilon)\,\mathrm{d}\epsilon = \frac{m_e}{e}u\delta u\int_0^\infty \epsilon\frac{\partial n_0}{\partial\epsilon}\,\mathrm{d}\epsilon$$

and integrating by parts,

$$\int_0^\infty \epsilon\frac{\partial n_0}{\partial\epsilon}\,\mathrm{d}\epsilon = \epsilon n_0(\epsilon)|_0^\infty - \int_0^\infty n_0(\epsilon)\,\mathrm{d}\epsilon = 0 - 0 - 1 = -1$$

we have

$$\delta\varepsilon_{\text{med}} = -\frac{m_e}{e}u\delta u$$

which is the variation of electron kinematic energy per particle.

VII. Current Anisotropy

To clarify the role of the matrix $\hat{\omega}$, let us consider the configuration with the magnetic field oriented in the z direction, $\mathbf{B} = (0, 0, B)$. For this condition, and defining

$$\beta = \frac{eB}{\nu_e m_e} \qquad \alpha = \frac{\beta}{\nu_e(1+\beta^2)} \qquad \gamma = \frac{1}{\nu_e(1+\beta^2)} \tag{A53}$$

we have

$$\hat{\omega} = \frac{1}{\nu_e(1+\beta^2)}\begin{pmatrix} 1 & \beta & 0 \\ -\beta & 1 & 0 \\ 0 & 0 & 1+\beta^2 \end{pmatrix} = \begin{pmatrix} \gamma & \alpha & 0 \\ -\alpha & \gamma & 0 \\ 0 & 0 & 1 \end{pmatrix} \tag{A54}$$

Referring to the expression of $\mathbf{n}_1$ in Eq. (A52) and considering that the current density as

$$\mathbf{J} = N_e e\mathbf{v}_{\text{d}} = N_e e\int_0^\infty \mathbf{n}_1\,\mathrm{d}\epsilon \tag{A55}$$

for $\mathbf{E} = (0, \mathrm{E}, 0)$, the Hall current is oriented in the x direction and its value is given by

$$j_{\text{Hall}} = -\frac{2N_e e^2}{3m_e}\int_0^\infty \epsilon\sqrt{\epsilon}\frac{\partial}{\partial\epsilon}\frac{n}{\sqrt{\epsilon}}\alpha E\,\mathrm{d}\epsilon \tag{A56}$$

Acknowledgments

This paper was partially supported by Agenzia Spaziale Italiana-Configurazioni Aerotermodinamiche Innovative per Sistemi di Trasporto Spaziale (ASI-CAST). The authors want to thank the referees and the Associate Editor Deborah Levin for the useful suggestions.

References

[1] Abe, M., Okuno, Y., and Yamasaki, H., "Characteristics of Shock Wave in an MHD Channel Flow," AIAA Paper 2001-3099, 2001.

[2] Bityurin, V., Bocharov, A., and Lineberry, J., "MHD Flow Control in Hypersonic Flight," AIAA Paper 2005-3225, May 2005.

[3] Leonov, S., Bityurin, V., Savelkin, K., and Yarantsev, D., "Effect of Electrical Discharge on Separation Processes and Shocks Position in Supersonic Airflow," AIAA Paper 2002-0355, 2002.

[4] Bobashev, S. V., Golovachov, Y. P., and Van Wie, D. M., "Deceleration of Supersonic Plasma Flow by an Applied Magnetic Field," *Journal of Propulsion and Power*, Vol. 19, No. 4, 2003, pp. 538–546.

[5] Macheret, S. O., Shneider, M. N., and Miles, R. B., "Magneto-hydrodynamic and Electrohydrodynamic Control of Hypersonic Flows of Weakly Ionized Plasmas," *AIAA Journal*, Vol. 42, No. 7, 2004, pp. 1378–1387. doi:10.2514/1.3971

[6] Adamovich, I. V., Rich, J. W., and Nelson, G. L., "Feasibility Study of Magnetohydrodynamics Acceleration of Unseeded and Seeded Airflows," *AIAA Journal*, Vol. 36, No. 4, 1998, pp. 590–597.

[7] Borghi, C. A., Carraro, M. R., and Cristofolini, A., "Analysis of Magnetoplasmadynamic Interaction in the Boundary Layer of a Hypersonic Vehicle," *Journal of Spacecraft and Rockets*, Vol. 42, No. 1, 2005, pp. 45–50. doi:10.2514/1.4031

[8] Borghi, C. A., Carraro, M. R., Cristofolini, A., Veefkind, A., Biagioni, L., Fantoni, G., Passaro, A., Capitelli, M., and Colonna, G., "Magneto-Hydrodynamic Interaction in the Shock Layer of a Wedge in a Hypersonic Flow," *IEEE Transactions on Plasma Science*, Vol. 34, No. 5, 2006, pp. 2450–2463. doi:10.1109/TPS.2006.883377

[9] Borghi, C. A., Cristofolini, A., Carraro, M. R., Gorse, C., Colonna, G., Passaro, A., and Pagannucci, F., "Magneto-Hydrodynamic Interaction in the Shock Layer of a Wedge in a Hypersonic Flow," AIAA Paper 2006-8050, Dec. 2006.

[10] Colonna, G., and Capitelli, M., "The Effects of Electric and Magnetic Fields on High Enthalpy Plasma Flows," AIAA Paper 2003-4036, May 2003.

[11] Colonna, G., and Capitelli, M., "Self-Consistent Model of Chemical, Vibrational, Electron Kinetics in Nozzle Expansion," *Journal of Thermophysics and Heat Transfer*, Vol. 15, No. 3, 2001, pp. 308–316.

[12] Colonna, G., and Capitelli, M., "The Influence of Atomic and Molecular Metastable States in High Enthalpy Nozzle Expansion Nitrogen Flows," *Journal of Physics D: Applied Physics*, Vol. 34, No. 12, 2001, pp. 1812–1818. doi:10.1088/0022-3727/34/12/308

[13] Colonna, G., Tuttafesta, M., and Giordano, D., "Numerical Methods to Solve Euler Equations in One-Dimensional Steady Nozzle Flow," *Computer Physics Communications*, Vol. 138, No. 3, 2001, pp. 213–221. doi:10.1016/S0010-4655(01)00211-9

[14] Colonna, G., "Step Adaptive Method for Vibrational Kinetics and Other Initial Value Problems," *Supplemento ai Rendiconti del Circolo Matematico di Palermo*, Series II, Vol. 57, 1998, pp. 159–163.

[15] Mitchner, M., and Kruger, C. H. J., *Partially Ionized Gases*, Wiley, New York, 1973.

[16] Golant, V. E., Zilinskij, A. P., and Sacharov, I. E., *Fundamentals of Plasma Physics*, Wiley, New York, 1980.

[17] Colonna, G., Gorse, C., Capitelli, M., Winkler, R., and Wilhelm, J., "The Influence of Electron-Electron Collisions on Electron Energy Distribution Functions in N_2 Post Discharge Conditions," *Chemical Physics Letters*, Vol. 213, No. 1, 1993, pp. 5–9. doi:10.1016/0009-2614(93)85410-P

[18] Rockwood, S. D., "Elastic and Inelastic Cross Sections for Electron-Hg Scattering from Hg Transport Data," *Physical Review A*, Vol. 8, No. 5, 1973, pp. 2348–2358.